Confined Steel Brace for Earthquake Resistant Design

CHRISTOPHER C. HIGGINS and JAMES D. NEWELL

In the United States, there is a shift toward performance-based design of structures and increased demand for higher structural performance during earthquakes. Building owners are increasingly interested in immediate occupancy following large earthquakes and want to mitigate economic losses due to structural damage during a seismic event. One method for protecting structures and achieving higher performance levels is the application of passive energy dissipaters. Viscous, viscoelastic, and metallic dampers are passive devices currently used to increase the performance level of structures during seismic events. While viscous and viscoelastic dampers are becoming more common, application of metallic dampers has recently begun to increase in the U.S.

Metallic dampers rely on the hysteretic damping capacity of the metal component of the device and the post-yield properties of the metallic elements to provide the design level of ductility and energy dissipation. The metallic damper system utilizes the inelastic deformation allowance of the *Uniform Building Code* (ICBO, 1997) by providing elements designed to dissipate the input seismic energy through controlled cyclic inelastic deformations.

One such metallic damper, a tension-compression yielding brace or buckling-restrained brace (BRB) termed the Unbonded Brace™ (UBB) has been developed by Nippon Steel of Japan (Aiken, Clark, Tajirian, Kasai, Kimura, and Ko, 2000; Black, Makris, and Aiken, 2002; Wantanabe, 1992; Wantanabe, Hitomi, Saeki, Wada, and Jujimoto, 1988). Other BRBs have been developed and tested in the U.S. (Merritt, Uang, and Benzoni, 2003a; Merritt, Uang, and Benzoni, 2003b; Merritt, Uang, and Benzoni, 2003c). Japanese practice typically incorporates UBBs as separate passive energy dissipation elements in moment resisting frames. In this application the UBB devices act as metallic dampers. U.S. practice has been to use buckling-restrained braces to replace conventional brace members in braced frame construction. In this application the buckling-restrained brace serves as a ductile brace with improved tension/compression characteristics as compared with conventional bracing members. The UBB relies upon a structural tube filled with mortar that confines a steel yielding core. A debonding agent is applied between the concrete and steel allowing space for Poisson's effect and reducing shear stress transfer between the steel yielding core, mortar, and confining tube. The mortar provides buckling resistance that allows the steel core to yield in compression as well as in tension, thereby permitting stable and symmetric hysteretic energy dissipation capacity under fully reversed cyclic loading. To ensure that the damper does not buckle in the first mode, the UBB must satisfy the following condition:

$$\frac{\pi^2 EI}{L^2} \geq \alpha P \tag{1}$$

where

E = Young's Modulus
I = moment of inertia of the outer confining tube
L = brace length, taken as work-point to work-point
α = global buckling factor of safety
P = design axial load including the effects of strain hardening (Wantanabe, 1992)

When the conditions of this equation are met, the external structural tube will provide the necessary global buckling resistance and enable the steel core to yield in compression instead of global brace buckling in first mode. Testing and analysis conducted to assess the performance of BRBs indicated the device provides stable, reasonably symmetric hysteretic energy dissipation of the input cyclic loading (Aiken and others, 2000; Black and others, 2002; Tremblay, Degrange, and Blouin, 1999; Wantanabe, 1992; Wantanabe and others, 1988).

Christopher C. Higgins is assistant professor, department of civil, construction and environmental engineering, Oregon State University, Corvallis, OR.

James D. Newell is graduate student researcher, department of structural engineering, University of California, San Diego, La Jolla, CA, and formerly graduate research assistant, department of civil, construction and environmental engineering, Oregon State University, Corvallis, OR.

Buckling-restrained braced frames (BRBF) with UBBs have seen over 200 Japanese applications since 1987 (Black and others, 2002) and are gaining increased acceptance as a seismic force resisting system (SFRS) by the U.S. structural engineering community. BRBFs have been used in about 30 U.S. projects to date, including both new and retrofit construction. Most applications have used imported Nippon Steel UBBs from Japan. Currently, no adopted U.S. building code provisions exist for BRBF design. Recommended provisions have been developed by a joint American Institute of Steel Construction/Structural Engineers Association of California (AISC/SEAOC) committee, and this work has been incorporated into the 2003 *NEHRP Recommended Provisions for Seismic Regulation of New Buildings and Other Structures* (FEMA, 2003) and will be incorporated into the 2005 AISC *Seismic Provisions for Structural Steel Buildings*.

This paper addresses an economical, low-yield force alternative form of BRB in which the mortar of the UBB is replaced with confined non-cohesive material. This non-cohesive material provides buckling resistance of the core, enabling the device to yield in compression and in tension. Confined Yielding Braces (CYBs) provide benefits including economical use of standard materials, for example, ASTM A36 steel bar stock for the yielding core and ASTM A53A steel pipe for the confining tube. Further, this new device offers simplified connection design and detailing, opens the market for non-proprietary U.S. fabrication of CYBs using no patented technologies, offers applicability to a wider range of building structures as the brace yield force levels under investigation are lower than are currently available, and simplified design of the damper device because no debonding layer is required.

EXPERIMENTAL PROGRAM

Test Specimens

Small scale experimental CYB tests were carried out at Clarkson University (Higgins and Newell, 2001; Higgins and Newell, 2002). Test results indicated relatively stable and symmetric hysteretic damping with a reduced scale device. The current testing program was therefore undertaken to characterize large-scale CYB performance and establish design guidelines for future application of CYBs as a SFRS in structures.

In this research, two different yield force levels were investigated: 125 kip (556 kN) and a 50 kip (222 kN) yield force levels. These yield force levels correspond to brace seismic force demand in typical one to three story buildings and would represent a reduced scale device for larger structures. A dogbone and perforated yielding core configuration were tested at each force level. The CYB configurations, illustrated in Figure 1, consist of a steel yielding core element within a steel pipe filled with a confined non-cohesive material. The non-cohesive material takes the place of the mortar used in the UBB in providing lateral stability to the yielding core. Specimen cross-sections are shown in Figure 2. A constant confining material volume was maintained with steel end caps and ½ in. (12.70 mm) diameter A193 B-7 high-strength threaded rod. Threaded rods were tensioned to 5 kips (22.2 kN) each, as measured by bolt load cells, to provide confining pressure. The use of threaded rods and a removable end cap also facilitated the removal of confining material for post-event yielding core inspection and repair/replacement while reusing major portions of the device.

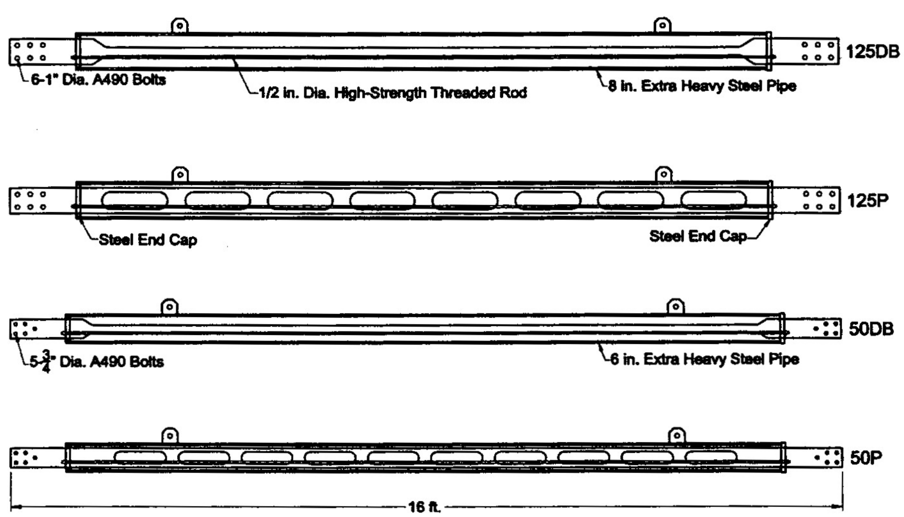

Fig. 1. CYB configurations.

To determine realistic brace geometry for testing, typical frame member sizes and dimensions were considered. Columns were assumed to be W14 sections and beams were assumed to be W21 sections. A full-scale specimen yielding core length of 16 ft (4.88 m) was selected for a single diagonal brace in a typical bay with column-to-column centerline spacing of 15 ft (4.57 m), beam-to-beam centerline spacing of 13 ft (3.96 m) and considering the gusset plate beam-to-column-to-brace connection, as illustrated in Figure 3.

The yielding core reduced cross-sectional area was calculated based on the desired yield force and material properties determined from tension coupon testing. The dogbone configuration, with a reduced width yielding core segment and unreduced width connection/transition region, is typical of current BRBs. The perforated configuration has the potential for greater design variation in the yield force and stiffness of the device by varying the geometric properties, and was also investigated. The legs of different perforations could be fabricated to different lengths,

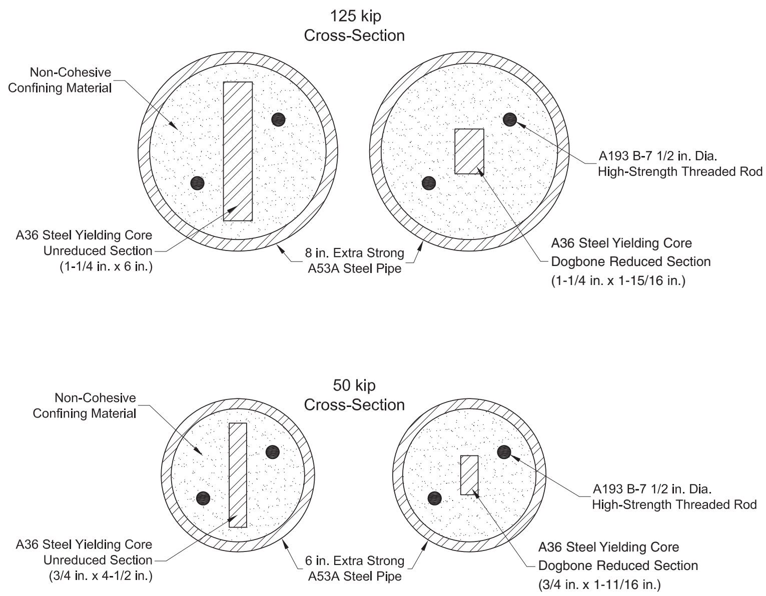

Fig. 2. CYB cross-sections.

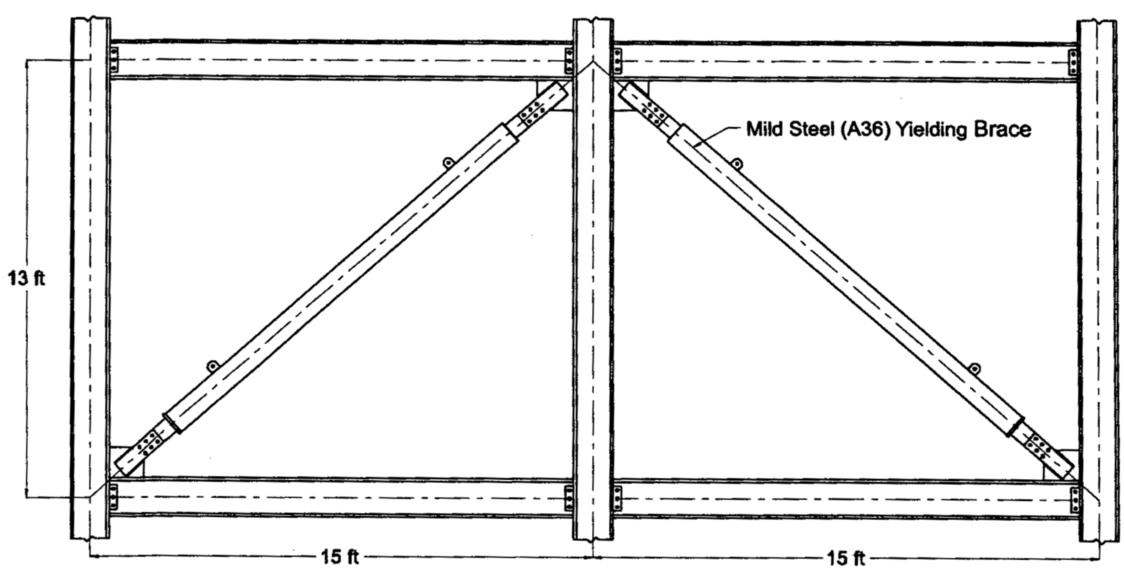

Fig. 3. Frame geometry with CYB.

cross-sectional areas or tapered allowing for tailoring of device performance. Fabrication costs for the dogbone and perforated configurations were equal for a given yield force CYB.

Specimens were identified by yield force level, yielding core configuration, and specimen identification number. For example, 125DB-1 was a 125 kip (556 kN) yield force, dogbone configuration, and specimen identification number 1. 50P-2 was a 50 kip (222 kN) yield force, perforated configuration, and specimen identification number 2.

The 125 kip yield force dampers consisted of $1\frac{1}{4}$ in. (31.75 mm) by 6 in. (152.40 mm) A36 steel bar stock with a yield stress (F_y) of 51.8 ksi (357.2 MPa) and an ultimate stress (F_u) of 72.1 ksi (497.1 MPa), based on tension coupon testing. The reduced cross-sectional area of the 125DB specimen was 2.422 in.^{2} (1562.6 mm^2), and the reduced cross-sectional area of each leg of the 125P specimen was 1.211 in.^{2} (781.3 mm^2), resulting in an area for both legs equivalent to that of the dogbone specimen. Length of individual perforation legs was 11 in. (279.40 mm) with a 2.3 factor of safety against buckling assuming pinned ends at the ends of the legs. Yielding core geometry for all specimens is shown in Figure 4. Two $\frac{3}{4}$ in. (25.4 mm) by 6 in. (152.40 mm) A36 splice plates were used to connect the yielding core to the reaction system. The confining tube for the 125 kip (556 kN) yield force specimens was an 8 in. (203.20 mm) extra heavy steel pipe (A53A) with a factor of safety against global buckling of 2.7 assuming pin-ended connections for the brace, work-point to work-point on the brace length, and considering the compressive stress of the yielding core including strain hardening.

The 50 kip (222 kN) yield force dampers consisted of $\frac{3}{4}$ in. (19.05 mm) by $4\frac{1}{2}$ in. (114.30 mm) A36 steel bar stock with a yield stress (F_y) of 39.5 ksi (272.4 MPa) and an ultimate stress (F_u) of 63.6 ksi (438.5 MPa). The reduced cross-sectional area of the 50DB specimen was 1.266 in.^{2} (816.7 mm^2), and the reduced cross-sectional area of each leg of the 50P specimen was 0.633 in.^{2} (408.4 mm^2) providing an area of both legs equivalent to that of the dogbone specimen. Length of individual perforation legs was 9 in. with a 2.4 factor of safety against buckling assuming pinned ends for individual legs. Yielding core geometry is shown in Figure 4. Two 1 in. (25.4 mm) by 6 in. (152.40 mm) A36 splice plates were used to connect the yielding core to the reaction system. The confining tube for the 50 kip (222 kN)

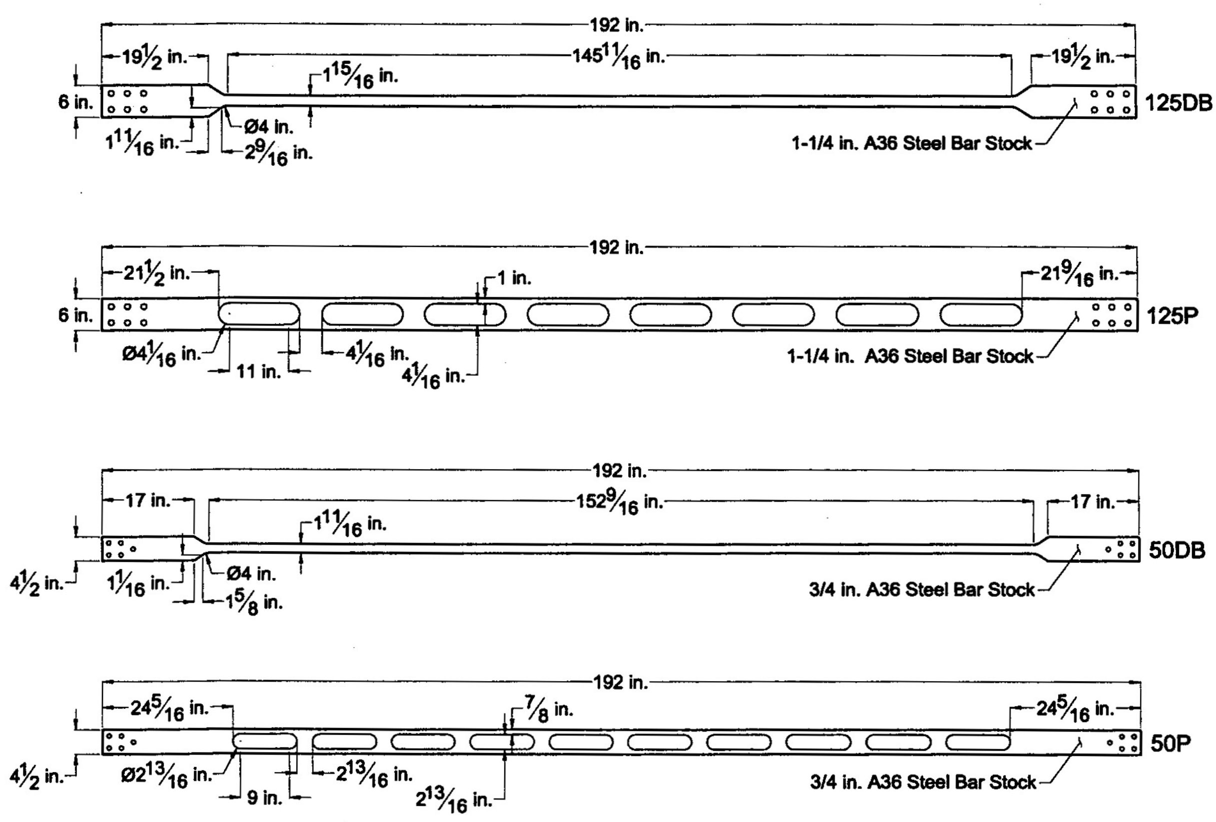

Fig. 4. Yielding core geometries.

Table 1. Yielding Core Properties

Specimen	Yield Stress F_y		Ultimate Stress F_u		Area of Reduced Cross-Section		Yield Force P_y		Yield Displacement Δ_{by}		Local Brace Stiffness K	
	(ksi)	(MPa)	(ksi)	(MPa)	(in.^{2})	(mm^2)	(kip)	(kN)	(in.)	(mm)	(kip/in.)	(kN/mm)
(1)	(2)		(3)		(4)		(5)		(6)		(7)	
125DB	51.8	357.2	72.1	497.1	2.422	1562.6	125	556	0.278	7.06	451	79.0
125P	51.8	357.2	72.1	497.1	2.422	1562.6	125	556	0.216	5.49	581	101.7
50DB	39.5	272.4	63.6	438.5	1.266	816.8	50	222	0.222	5.64	225	39.4
50P	39.5	272.4	63.6	438.5	1.266	816.8	50	222	0.174	4.42	287	50.3

yield force specimens was a 6 in. (152.40 mm) extra heavy steel pipe (A53A) with a factor of safety against buckling of 2.3 using previous assumptions.

Yielding core elastic stiffness and yield displacement values are summarized in Table 1 and take into account the unreduced sections of the yielding core that remain elastic after the reduced sections have yielded up to the first line of bolts.

Connections for both yield force levels were detailed as slip-critical bolted connections with Class A slip surfaces and fully-tensioned ASTM A490 high-strength structural bolts designed per the 1993 *Load and Resistance Factor Design Specification for Structural Steel Buildings* (AISC, 1993). Six (6) 1-in.-diameter (25.40 mm) A490 bolts were used for the 125 kip (556 kN) yield force specimens and five (5) $^3/_4$-in.-diameter (19 mm) A490 bolts were used for the 50 kip (222 kN) yield force specimens. Connections were designed to resist the ultimate strength (F_u) of the steel yielding core as determined from tension coupon testing and also taking into account the compressive overstrength factor of 1.1 typical of previously tested BRBs (Aiken and others, 2000). The net section of the connection was designed to remain elastic at a load equal to the yielding core ultimate tensile strength. Washers were used under both the head of the bolt and nut per RCSC *Specification for Structural Joints* (RCSC, 1994) for steel with a nominal yield stress less than 40 ksi (275.8 MPa).

Structural Test Matrix

Fourteen large-scale CYBs were tested to characterize device performance and investigate the influence of various parameters on behavior as shown in the test matrix, Table 2. The performance of different confining materials was investigated using the 125 DB specimens. Four different readily available aggregates were used as confining material: sand, pea gravel ($^1/_4$ in. (6.35 mm) minus gravel), $^3/_4$ in. (19.05 mm) to #4 (4.75 mm) gravel, and $^3/_4$ in. (19.05 mm) minus gravel (which consisted of equal parts of the above). Pea gravel was used as the confining material for all other specimens. Different configurations of perforation blocking (Figure 5) were tested with the 125P specimens to optimize performance and minimize lower modes of buckling for individual legs. A decreasing amplitude displacement history was compared to the typical increasing amplitude displacement protocol with the 50DB specimens. CYB performance when subjected to a random displacement history was evaluated with the 50P specimens with perforation blocking as shown in Figure 5.

Specimen Fabrication

The dogbone and perforated configuration yielding cores were fabricated using abrasive water jet cutting techniques. A 50,000 psi (344.75 MPa) water and garnet abrasive cutting stream was CNC controlled to cut the required configurations. Testing of both water jet and traditionally machined tension coupons did not indicate a change in the stress-strain behavior from the water jet cutting process for the 1$^1/_4$ in. (31.75 mm) A36 steel bar stock used for the 125 kip (556 kN) yielding cores.

The weight of confining material placed in the tube was calculated to achieve approximately 95 percent relative density. Actual confining material volumes, weights, and densities are given in Table 3. The tube was filled with confining material in a vertical orientation with the yielding core maintained in proper alignment. Confining material was placed in approximately 30 lb (0.13 kN) lifts and compacted internally with a pencil vibrator and/or externally with a 5 lb (0.02 kN) dead blow hammer on the outside of the confining tube. Method of compaction is included in Table 3. Sheet metal and spray foam crush-zones 6 in. (152.40 mm) in length were added to the dogbone yielding cores in the transition zone from reduced to unreduced cross

Table 2. Test Matrix

Specimen (1)	Parameter (2)
125DB[a]-1	Pea Gravel
125DB-2	Pea Gravel (Pencil Vibrator)
125DB-3	Sand
125DB-4	3/4" - #4 Gravel
125DB-5	3/4" - minus Gravel
125P[b]-1	All perforations spray foamed
125P-2	First perforation @ each end completely blocked, remaining perforations with spray foamed radius
125P-3	First 2 perforations @ each end completely blocked, remaining perforations with spray foamed radius
125P-4	First 2 perforations @ each end completely blocked, remaining perforations blocked with knockout minus 2 in. length (with cut in middle of knockout)
125P-5	First 2 perforations @ each end completely blocked, remaining perforations blocked with plate minus 2 in. length, minus 1/2 in. width
50DB-1	Increasing amplitude displacement protocol
50DB-2	Reverse displacement protocol from 2.0 Δ_{bm}
50P-1	Increasing amplitude displacement protocol
50P-2	Random displacement history

[a]DB - Dogbone configuration
[b]P - Perforated configuration

Table 3. Confining Material Properties

Specimen	Confining Material	Compaction Method	Weight of Confining Material		Volume of Voids		Confining Material Density	
			(lb)	(kN)	(ft^3)	(m^3)	(lb/ft^3)	(kN/m^3)
(1)	(2)	(3)	(4)		(5)		(6)	
125DB[a]-1	Pea Gravel	DBH[c]	412.00	1.83	3.88	0.1099	106.19	16.68
125DB-2	Pea Gravel	DBH/PV[d]	438.50	1.95	3.85	0.1090	113.90	17.89
125DB-3	Sand	DBH	382.50	1.70	3.86	0.1093	99.09	15.56
125DB-4	3/4" - #4 Gravel	DBH	400.00	1.78	3.88	0.1099	103.09	16.19
125DB-5	3/4" - minus Gravel	DBH	466.75	2.08	3.88	0.1099	120.30	18.89
125P[b]-1	Pea Gravel	DBH	361.75	1.61	3.46	0.0980	104.55	16.42
125P-2	Pea Gravel	DBH	390.25	1.74	3.66	0.1037	106.63	16.75
125P-3	Pea Gravel	DBH	375.75	1.67	3.59	0.1017	104.67	16.44
125P-4	Pea Gravel	DBH	356.00	1.58	3.46	0.0980	102.89	16.16
125P-5	Pea Gravel	DBH/PV	387.50	1.72	3.44	0.0974	112.65	17.69
50DB-1	Pea Gravel	DBH/PV	265.75	1.18	2.28	0.0646	116.56	18.31
50DB-2	Pea Gravel	DBH/PV	268.25	1.19	2.28	0.0646	117.65	18.48
50P-1	Pea Gravel	DBH/PV	236.00	1.05	2.10	0.0595	112.38	17.65
50P-2	Pea Gravel	DBH/PV	231.25	1.03	2.10	0.0595	110.12	17.30

[a]DB - Dogbone configuration
[b]P - Perforated configuration
[c]DBH - Dead blow hammer
[d]PV - Pencil vibrator

section to minimize compressive stiffening from the shoulders of the dogbone shaped yielding core bearing on the confining material. Perforated yielding cores were encased in sheet metal to maintain alignment of blocking material within individual perforations.

Structural Testing Setup

Specimens were tested in a horizontal configuration, Figure 6, with a structural steel reaction system at each end attached to the laboratory strong floor. Roller supports were provided at approximate third points of the confining tube to protect the test setup from any overall damper instability. The rollers provided negligible resistance to tube movement in the brace axial direction but prevented any excessive deformation in the transverse directions. Load was applied at a rate of 1.33 in./min (33.78 mm/min) with a 500 kip (2,224 kN) capacity servo-controlled hydraulic actuator. Specimen yielding core axial deformation was used as the feedback sensor for displacement control of the servo-

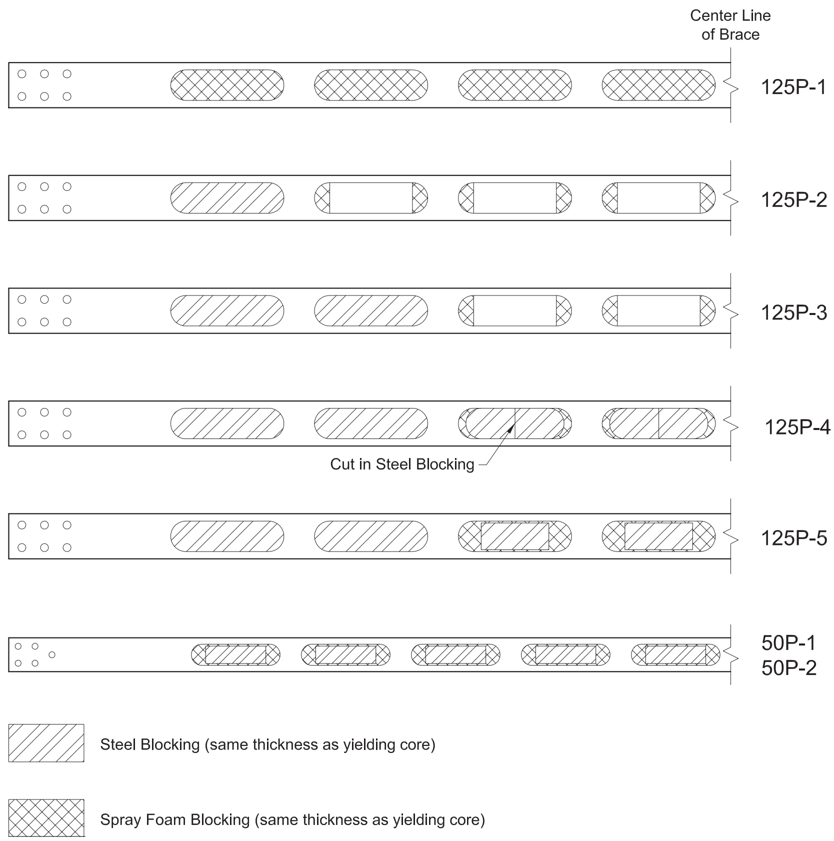

Fig. 5. CYB blocking configurations used with perforated specimens.

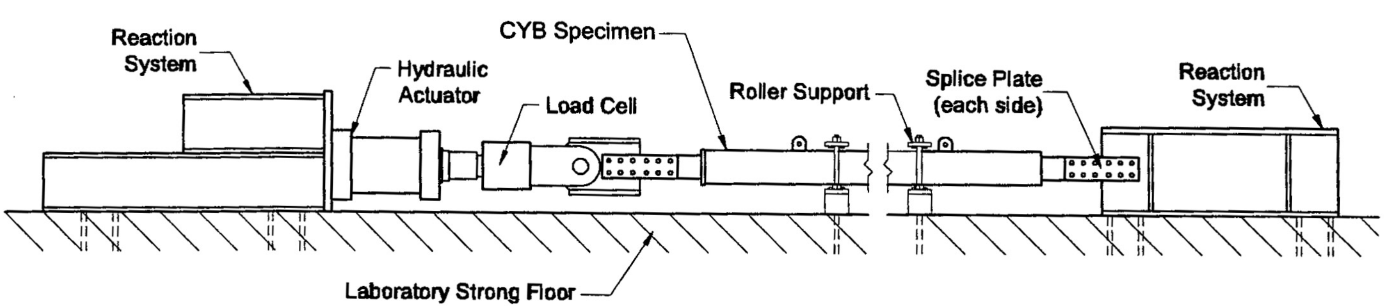

Fig. 6. Experimental setup.

hydraulic system. Instrumentation consisted of strain gages, displacement transducers, and a load cell in series with the specimen. Strain gages on the steel yielding cores and confining tube were used to measure axial strains and determine if bending was occurring within the elastic range of the gages. Two displacement sensors (string potentiometers) were used to measure overall yielding core deformation. Displacement values from these two sensors were averaged to remove any bending component due to brace end-rotation outside of the confining tube. Instrumentation layout for all sensors is detailed in Newell (2003). A PC-based data acquisition system was used to acquire data at a continuous rate of 5 Hz during testing.

Increasing Amplitude Displacement Protocol

The displacement protocol (Figure 7) was based on the guidelines of ATC 24 (ATC, 1992) and the AISC/SEAOC *Recommended Buckling-Restrained Brace Frame Provisions* (AISC/SEAOC, 2001). Increasing amplitude fully reversed cyclic axial displacement was applied until failure. Two cycles each were applied at 0.25 Δ_{by}, 0.50 Δ_{by}, and 0.75 Δ_{by}, where Δ_{by} equaled the yield displacement of the steel core. Six cycles at Δ_{by} were then applied. The remaining protocol was based on the design story drift of 1 percent (Δ_{bm}, 1.19 in. (30.23 mm) local brace displacement) on the frame geometry shown in Figure 3. Four cycles each were applied at deformation levels corresponding to 0.5 Δ_{bm}, 1.0 Δ_{bm}, and 1.5 Δ_{bm}. Two cycles were applied at 2.0 Δ_{bm} and higher deformation levels incremented by 0.5 Δ_{bm} to failure. Design story drift of 1 percent corresponded to the minimum recommended value for determination of Δ_{bm} (AISC/SEAOC, 2001) and was selected to represent a moderate earthquake demand for the initial experimental evaluation of large-scale CYB devices. The loading protocol developed for this testing also applied two cycles at 2.0 Δ_{bm} and higher deformation levels incremented by 0.5 Δ_{bm} to failure where the AISC/SEAOC protocol would return to 1.0 Δ_{bm} until a cumulative ductility value of 140 Δ_{by} was achieved. CYB specimens were therefore subjected to deformation demands greater than that resulting from the AISC/SEAOC loading protocol based on 1 percent story drift.

Random Displacement History Development

Specimen 50P-2 was subjected to multiple iterations of a random displacement history derived from nonlinear dynamic time-history analysis of a three-story BRBF building. The building modeled in this analysis is based on the work of Sabelli (2000) and the SAC model building design criteria. The SFRS consisted of eight BRBFs with four in each orthogonal direction. The building was designed for a site in metropolitan Los Angeles according to the 1997 *NEHRP Recommended Provisions for Seismic Regulation of New Buildings and Other Structures* (FEMA, 1997) and the 1997 *Uniform Building Code* (ICBO, 1997).

For analysis, one BRBF was modeled with an additional single column representing the secondary *P*-Δ load affect attributed to the BRBF. The horizontal stiffness contribution of this equivalent gravity framing column was neglected as is standard design practice. The frame model is shown in Figure 8 and member properties reported in Table 4.

Nonlinear dynamic time history analysis was conducted using the computer program PC-ANSR (Maison, 1992). Frame members were modeled as nonlinear beam-column elements. Beams were considered inextensible. Nodal dis-

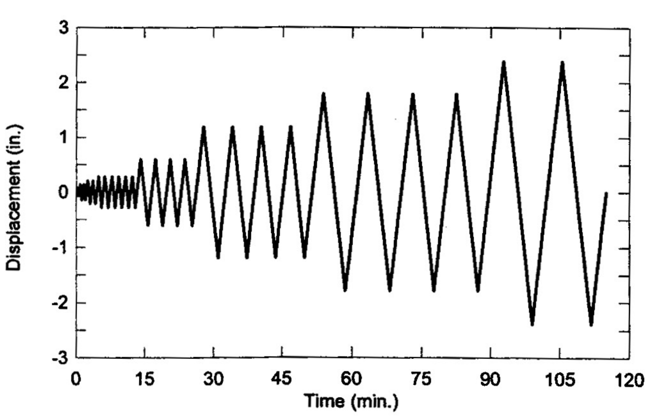

Fig. 7. Increasing amplitude displacement protocol imposed on most test specimens.

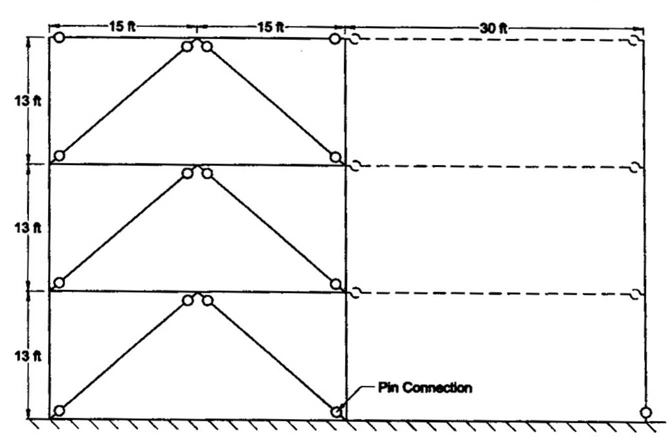

Fig. 8. Three-story BRBF model.

Table 4. Three-Story BRBF Model Member Properties

Story	Brace Yield Force		Horiz. Brace Stiffness		BF Column	BF Beam	Non-BF Columns (Minor Axis)							
	P_y		K_h				Side	Interior	Mech.	Perp. BF	ΣI_y		ΣZ_y	
	(kip)	(kN)	(kip/in.)	(kN/mm)							(in.^{4})	(mm^4)	(in.^{3})	(mm^3)
(1)	(2)		(3)		(4)	(5)	(6)	(7)	(8)	(9)	(10)		(11)	
3	117	520	588	103										
2	196	872	943	165	W12x96	W14x48	W14x48	W14x61	W14x74	W12x96	1,033	429,967,063	290	4,752,249
1	243	1081	1088	191										

placements within a story were set to be equivalent. Connections with gusset plates for brace attachment were modeled as rigid. The roof beam/column connections where no braces framed in were considered pinned (simple shear tab). All framing members were ASTM A992 steel, with a strain hardening modulus 5 percent that of Young's Modulus. Braces were modeled as nonlinear truss elements. ASTM A36 steel was assumed for the braces. The compressive yield stress was modeled as 110 percent of the tensile yield stress, based on previous buckling-restrained brace test results (Aiken and others, 2000). Brace cross-sectional area was calculated from the brace yield force given by Sabelli (2000) and a nominal yield stress of 36 ksi. An equivalent Young's Modulus was then calculated from this area and the required horizontal brace stiffness. A post-yield slope of 1 percent of the brace elastic stiffness was used, as determined from published UBB experimental testing load-displacement response (Aiken and others, 2000). Equivalent viscous damping of 5 percent was assumed for the structure per standard practice in the seismic design of steel structures and was applied as mass and initial stiffness proportional damping factors.

Ground motions considered (LA01-LA20) were developed for the SAC steel project (Woodward-Clyde Federal Services, 1997). The 20 earthquake records used are for a site in Los Angeles with a 10 percent probability of exceedence in 50 years. Nonlinear dynamic time history analysis was completed for the LA series earthquakes and the results analyzed to determine which event produced the greatest BRB demand. Of the 20 synthetic earthquake records, LA20 generated the highest BRB demand in terms of maximum brace displacement and cumulative ductility. First story compression dominated brace axial displacement time history response for LA20 is shown in Figure 9. This displacement history was simplified and scaled to develop a random displacement history (Figure 10). In the simplification, large peak-to-peak displacements were retained and smaller elastic cycles were neglected. Displacement values were scaled such that the maximum compressive displacement corresponded to 1 percent story drift for the frame geometry of Figure 3. This was done for consistency with the increasing amplitude protocol displacement demand and to scale the random displacement history demand from

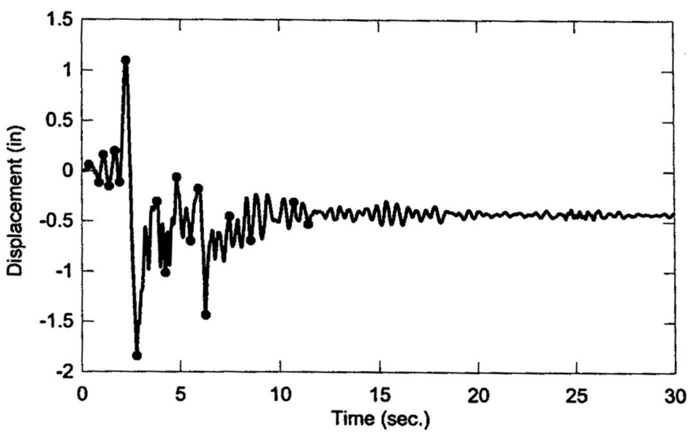

Fig. 9. First story BRB axial displacement time history for LA20.

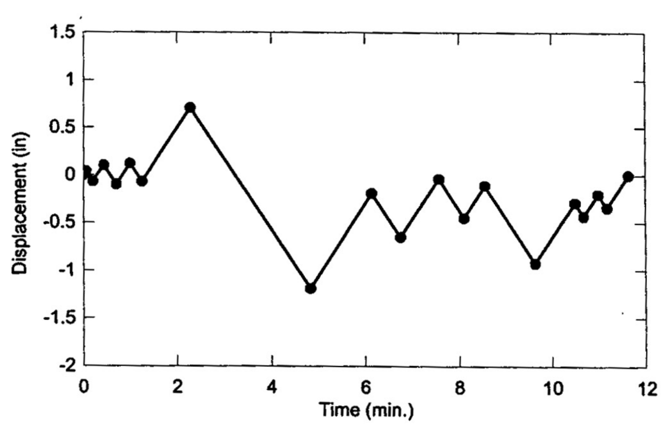

Fig. 10. Simplified random displacement history imposed on specimen 50 DB-2.

Table 5. CYB Performance Summary

Specimen	Max. Tensile Force T		Max. Compressive Force C		β	Max. Tensile Displacement		Max. Compressive Displacement		Total Energy Dissipated		Cumulative Ductility	Fracture On Cycle	1st Compressive Degradation On Cycle
	(kip)	(kN)	(kip)	(kN)	(C/T)	(in.)	(mm)	(in.)	(mm)	(kip-in.)	(kN-mm)	(Δ_{by})		
(1)	(2)		(3)		(4)	(5)		(6)		(7)		(8)	(9)	(10)
125DB[a]-1	151.6	674.3	154.7	688.1	1.02	2.404	61.06	2.452	62.28	5,230	590,881	176	1 @ 2.0 Δ_{bm}	2 @ 1.5 Δ_{bm}
125DB-2	155.8	693.0	163.5	727.2	1.05	2.394	60.81	2.074	52.68	6,165	696,517	183	2 @ 2.0 Δ_{bm}	2 @ 1.5 Δ_{bm}
125DB-3	145.8	648.5	95.5	424.8	0.66	4.177	106.10	1.705	43.31	2,051	231,720	125[c]	[e]	1 @ 0.5 Δ_{bm}
125DB-4	143.6	638.7	137.0	609.4	0.95	2.969	75.41	2.803	71.20	5,852	661,154	272	1 @ 3.0 Δ_{bm}	3 @ 0.5 Δ_{bm}
125DB-5	167.2	743.7	143.9	640.1	0.86	2.391	60.73	2.057	52.25	5,785	653,585	216	2 @ 2.0 Δ_{bm}	2 @ 1.5 Δ_{bm}
125P[b]-1	131.9	586.7	131.1	583.1	0.99	1.269	32.23	1.038	26.37	1,525	172,293	83[c]	4 @ 1.0 Δ_{bm}	1 @ 0.5 Δ_{bm}
125P-2	158.6	705.5	169.6	754.4	1.07	2.204	55.98	1.689	42.90	4,955	559,812	220	1 @ 2.0 Δ_{bm}	3 @ 1.0 Δ_{bm}
125P-3	159.9	711.2	182.4	811.3	1.14	2.364	60.05	2.342	59.49	5,858	661,832	261	1 @ 2.0 Δ_{bm}	2 @ 1.5 Δ_{bm}
125P-4	166.2	739.3	257.6	1145.8	1.55[c]	2.408	61.16	2.278	57.86	7,637	862,822	280	[e]	[f]
125P-5	167.1	743.3	252.9	1124.9	1.51[c]	2.410	61.21	2.095	53.21	6,792	767,355	236	[e]	[f]
50DB-1	64.6	287.3	68.8	306.0	1.07	1.816	46.13	1.660	42.16	1,957	221,100	182	3 @ 1.5 Δ_{bm}	4 @ 1.0 Δ_{bm}
50DB-2	68.0	302.5	78.2	347.8	1.15	2.356	59.84	2.344	59.54	1,230	138,964	101[c]	[e]	2 @ 1.5 Δ_{bm}
50P-1	67.0	298.0	73.3	326.0	1.09	1.804	45.82	1.715	43.56	1,639	185,173	195	2 @ 1.5 Δ_{bm}	2 @ 1.0 Δ_{bm}
50P-2	57.9	257.5	72.1	320.7	[d]	0.718	18.24	1.223	31.06	1,475	166,660	180	[e]	Iteration 3

[a]DB - Dogbone configuration
[b]P - Perforated configuration
[c]Does not meet AISC / SEAOC Provisions
[d]Unequal tensile and compressive displacements
[e]Limit state other than fracture
[f]Compressive Degradation not observed

the larger analytically modeled CYB to the smaller experimentally tested CYB. The random displacement history was applied at the same 1.33 in./min (33.78 mm/min) displacement rate as the increasing amplitude displacement history. Multiple iterations of this random displacement history were applied to specimen 50P-2. After each iteration, both load and displacement were returned to zero with an additional small inelastic displacement and elastic unloading.

EXPERIMENTAL RESULTS

Parameters Used for Comparison

AISC/SEAOC *Recommended Buckling-Restrained Brace Frame Provisions* (AISC/SEAOC, 2001) specify that the ratio of maximum compressive force to maximum tensile force (β) shall not exceed 1.3. This criterion serves to limit potential unbalanced forces and ensures reasonably symmetric hysteretic behavior. BRB demand from the increasing amplitude displacement protocol defined in the *AISC/SEAOC Provisions* is based on nonlinear dynamic time history analysis of buckling-restrained braced frame (BRBF) buildings (Sabelli, 2000). BRBs are required to achieve displacements corresponding to 1.5 Δ_{bm} (mean of Sabelli analysis) and cumulative ductilities of 140 Δ_{by} (mean plus one standard deviation of Sabelli analysis). These are believed to be conservative values and may be revised as more data becomes available (AISC/SEAOC, 2001).

Test Observations

Results for all specimens are summarized in Table 5. Displacements reported in hysteresis figures are the CYB yielding core axial displacement. Typically the majority of core displacement relative to the tube took place at the actuator end of the specimen. It is believed this was due to the resistance to tube movement provided by the small frictional force developed between the yielding core, confining material, and steel pipe.

Bolt slip was not observed, indicating adequate slip critical connection design. Detailing of Class-A slip surface eliminated the expense of sand-blasted faying surfaces and did not diminish CYB performance.

Yielding was distributed along the entire reduced section yielding core length for both the dogbone and perforated configurations as evidenced by uniform flaking of mill scale. Strain gages on the yielding core did not indicate bending (with the exception of 125DB-3) and showed balanced strains at instrumented locations up to the 3000 microstrain range limitation of the gages. Confining tube strain gages did not indicate significant bending.

The typical failure mechanism observed was fracture of the steel yielding core induced by increased tensile strains due to local high amplitude buckling at the actuator end of the specimen. This is an undesirable failure mechanism. It is anticipated that increasing the length of unreduced cross section within the confining tube would provide increased buckling resistance for this portion of the device. This would provide a larger unreduced yielding core surface area to be in contact with the confining material thereby limiting buckling and the associated bending induced tensile strains. This improved detail requires future experimental verification.

Confining Material Effects

CYB performance was determined to be highly dependent on the particle size of the confining material. 125DB specimens were tested using pea gravel, sand, $^3/_4$ in. (19.05 mm) to #4 gravel, and $^3/_4$ in. (19.05 mm) minus gravel.

Specimen 125DB-2 tested with pea gravel confining material provided reasonably stable and symmetric hysteretic response. The load-displacement curve for this specimen is shown in Figure 11. During the last few cycles of compressive displacement local large-amplitude yielding core buckling took place within the confining tube near the actuator end of the specimen. The resulting compressive degradation can be observed in the hysteretic response. Reduced tension capacity of the yielding core was also observed during reloading in tension and straightening of the local large-amplitude buckling. The β value of 1.05 is well within the suggested 1.3 limit and in line with a compressive overstrength of 1.1 typical of UBBs. A total of 6,165 kip-in. (696 517 kN-mm) of energy was dissipated by the device. The cumulative ductility of 183 Δ_{by} exceeded the 140 Δ_{by} requirement of the *AISC/SEAOC Provisions*.

Pea gravel confining material was also used for specimen 50DB-1. Figure 12 shows reasonably stable and symmetric dissipation of 1,957 kip-in. (221 100 kN-mm) of energy. The capacity reduction observed in the last few cycles of displacement was similar to that explained above for specimen 125DB-2. The β value was 1.07 and a cumulative ductility of 182 Δ_{by} was achieved. The smaller yield force device dissipated proportionally less energy but still achieved approximately the same cumulative ductility as 125DB-2.

Sand confining material did not adequately prevent the yielding core (125DB-3) from translating through the confining material. As a result the core buckled in approximately the fourth mode in the weak direction and second mode in the strong direction. The load-displacement curve (Newell, 2003) showed buckling with significant pinching of the hysteresis loops. Sand confining material for this specimen geometry does not provide sufficient confinement to enable stable and symmetric hysteretic damping.

Testing with $^3/_4$ in. (19.05 mm) to #4 gravel resulted in significant confining material crushing and considerable localized buckling at the ends of the reduced section of specimen 125DB-4. Compressive degradation was observed significantly earlier than with pea gravel or $^3/_4$ in. (19.05 mm) minus gravel confining material (cycle 3 @ 0.5 Δ_{bm} vs. cycle 2 @ 1.5 Δ_{bm}). The $^3/_4$ in. (19.05 mm) to #4

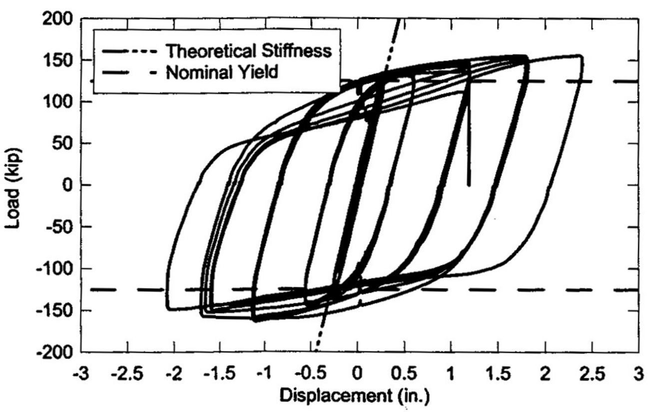

Fig. 11. Specimen 125DB-2 hysteresis.

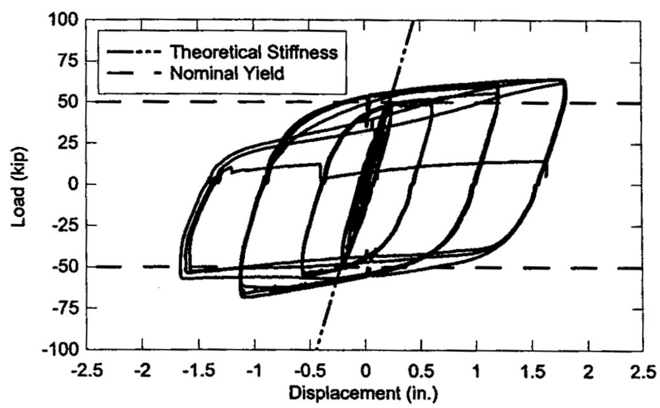

Fig. 12. Specimen 50DB-1 hysteresis.

gravel is not an optimal confining material for this specimen geometry.

Specimen 125DB-5 tested with 3/4 in. (19.05 mm) minus gravel confining material performed similar to specimen 125DB-2 confined with pea gravel. The larger aggregate locks together preventing translation of particles, with fines filling voids. No significant benefit was observed by using the 3/4 in. (19.05 mm) minus gravel. Pea gravel was used as the confining material for the remaining tests, and the costs associated with producing the 3/4 in. (19.05 mm) minus gravel blend were avoided.

Testing of different confining material indicated that particle size and shape must be such that localized crushing of the confining material does not create a significant volume loss, and that there is adequate particle interlock so that the yielding core cannot translate through the confining material.

Perforation Blocking Effects

Specimen 125P-1 was tested with perforations filled with spray foam to prevent the yielding core perforation ends from bearing on the pea gravel confining material. Desirable structural performance was not achieved, with the legs of the first perforation at the actuator end buckling into the void space. Abrupt stiffening occurred when the buckled legs came into contact with each other.

Following the poor performance of specimen 125P-1, different configurations of perforation blocking were investigated to prevent buckling of perforation legs. Further, design factors of safety against buckling of legs should be increased. Combinations where the complete width of the first two perforations at each end and partial width (void space width minus 1/2 in.) of the remaining perforations were blocked with steel plate provided the best performance. Future testing may confirm that perforation blocking could be completely avoided by detailing shorter perforation leg lengths, while still achieving large ductility.

Reasonably stable and symmetric hysteretic behavior is shown in Figure 13, for specimen 125P-5. The first two perforations at each end were completely blocked with the original knockout from water jet cutting. Remaining perforations were blocked using steel plate 2 in. (50.8 mm) shorter and 1/2 in. (12.7 mm) narrower than the perforation dimensions. The compressive elastic stiffness for this blocked configuration was 845 kip/in. (148 kN/mm), which was 1.45 times greater than the compression stiffness with no perforation blocking. This accounts for the compressive stiffening observed in the hysteresis curve. The β value of 1.51 is above the AISC/SEAOC 1.3 limit. Future detailing of shorter legs would eliminate the need for perforation blocking and the associated compressive stiffening. A total of 6,792 kip-in. (696 517 kN-mm) of energy was dissipated by the device. A cumulative ductility of 236 Δ_{by} was achieved before testing was suspended to prevent damage to the reaction system from the high compressive forces.

Specimen 50P-1 was tested with the first two perforations at each end blocked with a steel plate 1 in. (25.4 mm) shorter and equal in width to the perforation dimension. Remaining perforations were blocked with steel plates 1 in. (25.4 mm) shorter and 1/2 in. (12.7 mm) narrower than the perforation dimension. The hysteresis curve (Figure 14) indicates reasonably stable and symmetric hysteretic damping. Compressive stiffening (observed in specimen 125P-5) was eliminated by not blocking the full length of end perforations. The weak direction of each perforation leg was in the out-of-plane direction, and buckling was observed in the out-of-plane direction and thus not restrained by perforation blocking. This specimen dissipated 1,639 kip-in.

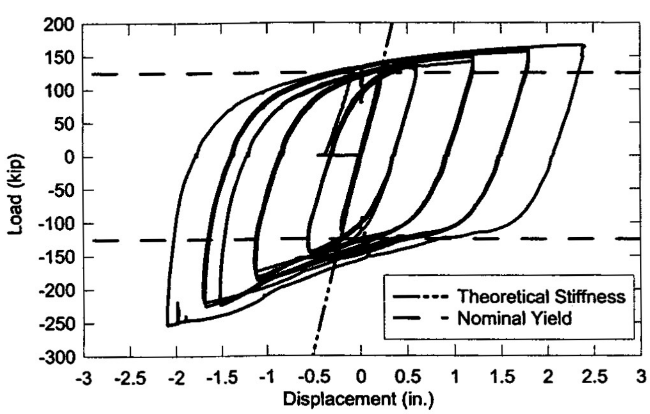

Fig. 13. Specimen 125P-5 hysteresis.

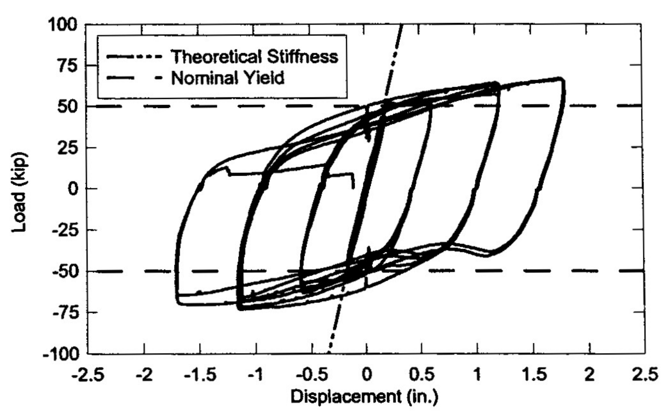

Fig. 14. Specimen 50P-1 hysteresis.

Table 6. Random Displacement History Iteration Comparison

Iteration	Max. Tensile Force T		Max. Compressive Force C		β	Max. Tensile Displacement		Max. Compressive Displacement		Total Energy Dissipated		Cumulative Ductility
	(kip)	(kN)	(kip)	(kN)	(C/T)	(in.)	(mm)	(in.)	(mm)	(kip-in.)	(kN-mm)	(Δ_{by})
(1)	(2)		(3)		(4)	(5)		(6)		(7)		(8)
1	56.4	250.8	65.1	289.4	1.15	0.718	18.24	1.176	29.87	230	26,039	24.0
2	53.8	239.3	72.1	320.9	1.34	0.719	18.26	1.186	30.12	223	25,186	24.6
3	56.9	253.1	70.0	311.5	1.23	0.724	18.39	1.185	30.10	211	23,891	24.3
4	57.9	257.7	65.5	291.3	1.13	0.726	18.44	1.188	30.18	196	22,134	24.3
5	57.6	256.1	63.0	280.3	1.09	0.727	18.47	1.183	30.05	186	20,990	24.4
6	57.2	254.3	62.0	275.9	1.09	0.727	18.47	1.186	30.12	179	20,233	24.5
7	55.8	248.0	58.4	259.7	1.05	0.692	17.58	1.149	29.18	159	18,019	22.8
8	54.3	241.4	58.4	259.6	1.08	0.698	17.73	1.132	28.75	90	10,167	11.5
									Total	1474	166,659	180.4

(185 173 kN-mm) of energy. The β value was 1.09 and a cumulative ductility of 195 Δ_{by} was achieved.

Decreasing Amplitude Displacement History

A decreasing amplitude displacement history was applied to specimen 50DB-2. One cycle at 2.0 Δ_{bm} (2 percent story drift) was followed by two cycles at 1.5 Δ_{bm}. Yielding core fracture was observed on the subsequent cycle at 1.0 Δ_{bm}. The energy dissipated and cumulative ductility were 1,230 kip-in. (138 964 kN-mm) and 101 Δ_{by}, respectively. These values are less than those of specimen 50DB-1 subjected to the increasing amplitude displacement protocol. However, for specimen 50DB-2 the largest single excursion displacement was 0.5 Δ_{bm} larger. This indicates that device performance has some dependence on applied displacement history. This observation is unique to CYB devices due to local crushing of confining material and rearrangement of particles during cycle loading. The increasing amplitude displacement protocol does not adequately indicate performance capability of CYBs for large excursions due to damage accumulated at lower displacement amplitudes. The devices can sustain very large excursions when sequenced at the beginning of the record before local crushing of confining material has occurred.

Random Displacement History

Specimen 50P-2 was subjected to the random displacement history derived from nonlinear time-history analysis as described previously. Seven complete iterations of the random displacement and an eighth iteration up to the point of maximum compressive displacement were applied. Loading was suspended at maximum compressive displacement to examine the yielding core in that state. Buckling and compressive stiffening was observed in the hysteresis curve (Figure 15). Based on visual observation after removal of the core plate, local buckling of the core against the confining tube resulted in the post-buckling compressive stiffening. Figure 16 presents each individual iteration of random displacement history and shows minor progressive degradation in CYB performance. There was a gradual decrease in the energy dissipated per iteration (Table 6) due to pinching of the hysteresis loops. Cumulative ductility values per iteration however do not capture the performance degradation because the same displacement amplitudes were achieved, but at lower axial forces. Therefore, performance specifications should include not only cumulative ductility and tension/compression ratios, but also measures of per-

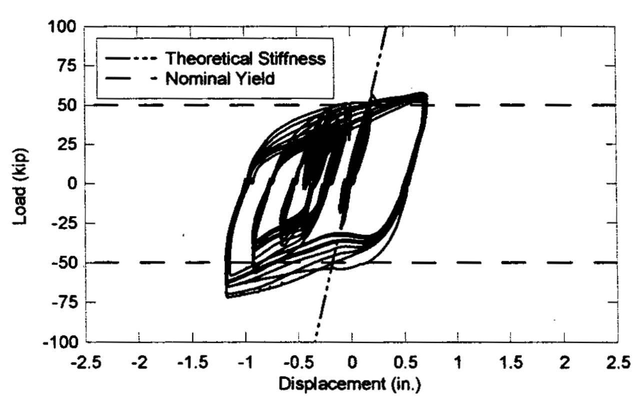

Fig. 15. Specimen 50P-2 hysteresis.

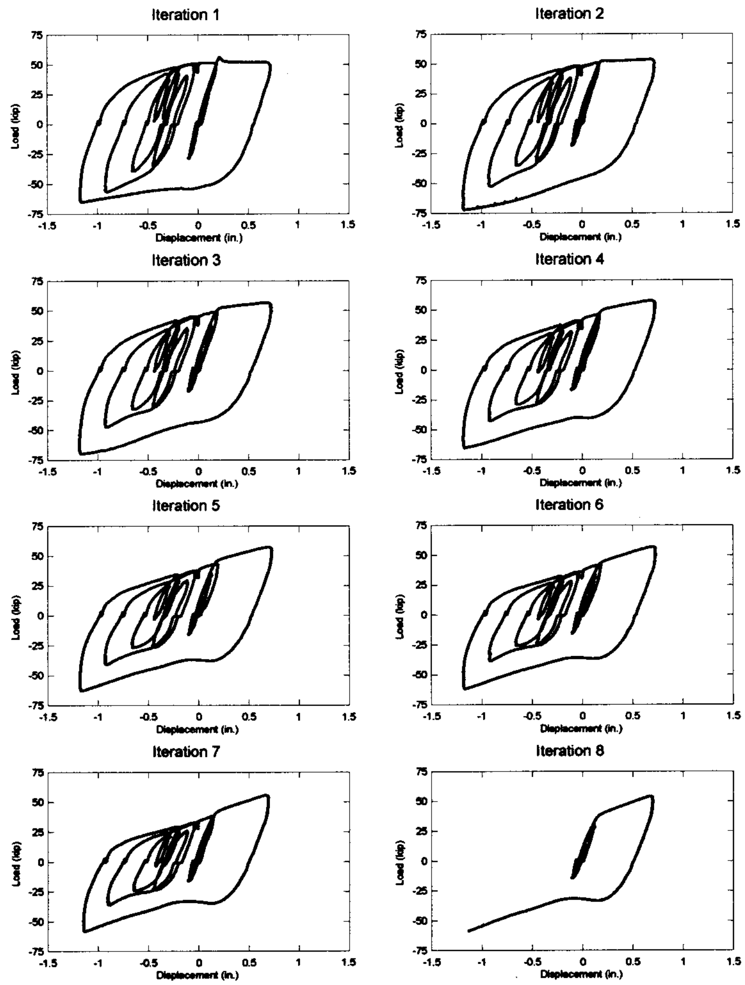

Fig. 16. Specimen 50P-2 hysteresis for each iteration of imposed random displacement history.

centage change in energy dissipation or secant stiffness on subsequent cycles of similar amplitude to ensure that local buckling behavior, possible with confining materials other than concrete, do not significantly degrade device performance.

Experimental results for specimen 50P-2 were compared with a time-history response for a single CYB subjected to the imposed random displacement history. Brace model properties were determined in the same manner as the three story building analysis. When compared to actual CYB performance, equal compressive and tensile yield strengths more accurately reflected experimental results. An efficiency factor of 80 percent was applied to Young's Modulus to better represent CYB elastic stiffness. Also, a strain hardening modulus of 7.5 percent was observed to more accurately reflect CYB post-yield stiffness. Experimental and analytical results are illustrated in Figure 17. The energy dissipated by specimen 50P-2 iteration 2 was 223 kip-in. (25,186 kN-mm) while the analytical model dissipated 170 kip-in. (19,206 kN-mm). The analytical model underestimated the energy dissipation capacity of the CYB.

The response of the three-story building model was assessed using the experimental CYB properties to determine if the imposed random displacement history was a reasonable representation of the model BRB demand. Analysis with experimental CYB properties resulted in similar cumulative brace displacement demand.

CONCLUSIONS

A new type of tension-compression yielding brace or buckling-restrained brace has been investigated and tested for seismic applications. The Confined Yielding Brace consists of a steel yielding core element within a structural tube filled with non-cohesive material. This non-cohesive material is placed under a normal confining force to provide buckling resistance of the core, enabling the device to yield in compression without global buckling of the brace. The testing program examined the effects of different confining material, perforation blocking configurations, and random displacement histories. Based on Confined Yielding Braces test results, the following observations and conclusions are presented:

1. A properly designed, detailed, and constructed CYB device exhibits reasonably stable and symmetric hysteretic response under fully reversed cyclic loading.

2. Bolt slip was avoided with slip-critical bolted connections, Class-A slip surfaces, and fully-tensioned A490 high-strength structural bolts.

3. Confining material particle size and shape must be such that localized crushing of the confining material does not create a significant volume loss, while providing adequate particle interlock to limit yielding core translation through the confining material.

4. Gradual degradation on compressive cycles was observed when a CYB was subjected to multiple iterations of a random displacement history, although the performance as measured by cumulative ductility or energy dissipation did not diminish significantly even after the sixth iteration.

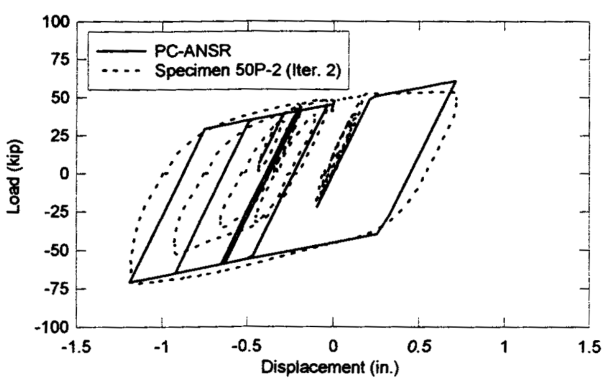

Fig. 17. Experimental and analytical force-deformation response for specimen 50P-2 during second iteration of imposed random displacement history.

5. Performance Specifications for CYBs should consider other quantitative measures to ensure reasonably stable and symmetric hysteretic response. Change in energy dissipation or secant stiffness on subsequent cycles of similar amplitude would provide an additional measure of device performance.

6. Nonlinear dynamic time history response calculated using experimentally determined CYB load-deformation properties resulted in cumulative brace displacement demand similar to that determined in development of the random displacement protocol using brace properties based on previous UBB testing.

7. The cross-sectional area and mechanical properties of the yielding core can be tailored to provide a device with the desired strength, stiffness, and yield surface properties. Use of the perforated configuration provides greater flexibility in design.

8. The CYB can provide performance similar to other types of buckling-restrained braces, and has the additional benefits of reduced cost, post-event inspection, design flexibility, reduced detailing, and can be designed and fabricated for relatively low-force applications.

The Confined Yielding Brace can provide a cost effective passive energy dissipation/buckling-restrained brace option that builds upon the strengths of the UBB. Desired structural performance properties of the CYB can be achieved by varying the cross-sectional area and mechanical properties of the steel core. Strength, stiffness, and yield surface properties can be adjusted using conventional grades of steel and different geometry of the steel core element, facilitating performance-based design objectives.

ACKNOWLEDGMENTS

This research was funded by the National Science Foundation (NSF) under Grant No. CMS-0099701 as part of the US-Japan Cooperative Research in Urban Earthquake Disaster Mitigation Program. Professor K. Kasai of the Tokyo Institute of Technology is the Japanese counterpart and Dr. Peter Chang was the program manager. Additional funding from the 2002 AISC/Klingelhofer Fellowship supported this research. Their support is gratefully acknowledged. The opinions, findings, and conclusions are those of the authors and do not necessarily reflect the views of NSF, AISC, or the individuals acknowledged above.

REFERENCES

American Institute of Steel Construction (AISC) (1993), *Load and Resistance Factor Design Specification for Structural Steel Buildings*, Chicago, December 1.

American Institute of Steel Construction / Structural Engineers Association of California (AISC/SEAOC) (2001), "Recommended Buckling-Restrained Braced Frame Code Provisions," Chicago.

Applied Technology Council (ATC) (1992), "Guidelines for Cyclic Seismic Testing of Components of Steel Structures," ATC-24, Redwood City, CA.

Aiken, I., Clark, P., Tajirian, F., Kasai, K., Kimura, I., and Ko, E. (2000), "Unbonded Braces in the United States-Design Studies, Large-Scale Testing and the First Building Application," *Proceedings of International Symposium on Passive Control*, pp. 203-217, Tokyo Institute of Technology, Tokyo, Japan.

Black, C., Makris, N., and Aiken, I. (2002), "Component Testing, Stability Analysis and Characterization of Buckling Restrained Braces," *Final Report to Nippon Steel Corporation*, Tokyo, Japan.

Federal Emergency Management Agency (FEMA) (1997), "NEHRP Recommended Provisions for Seismic Regulation of New Buildings and Other Structures," Washington, D.C.

FEMA (2003), "NEHRP Recommended Provisions for New Buildings and Other Structures," FEMA 450, Washington, D.C.

Higgins, C. and Newell, J. (2002), "Development of Two New Hysteretic Dampers," *Proceedings of the 7th U.S. National Conference on Earthquake Engineering*, Boston, July.

Higgins, C. and Newell, J. (2001), "Development of Economical Hysteretic Dampers," *Proceedings of the International Symposium on Passive Control*, Tokyo Institute of Technology, Tokyo, Japan, December.

International Conference of Building Officials (ICBO) (1997), "Uniform Building Code," Whittier, California.

Maison, B. (1992), "PC-ANSR A Computer Program for Nonlinear Structural Analysis," University of California, Berkeley, CA.

Merritt, S., Uang, C.M., and Benzoni, G. (2003a), "Subassemblage Testing of Corebrace Buckling-Restrained Braces," University of California, San Diego, Report No. TR-2003/01, La Jolla, CA.

Merritt, S., Uang, C.M., and Benzoni, G. (2003b), "Subassemblage Testing of Star Seismic Buckling-Restrained Braces," University of California, San Diego, Report No. TR-2003/04, La Jolla, CA.

Merritt, S., Uang, C.M., and Benzoni, G. (2003c), "Uniaxial Testing of Associated Buckling-Restrained Braces," University of California, San Diego, Report No. TR-2003/05, La Jolla, CA.

Newell, J. (2003), "Steel Confined Yielding Damper for Earthquake Resistant Design," M.S. Thesis, Oregon State University, Corvallis, OR.

Research Council on Structural Connections (RCSC) (1994), *Specification for Structural Joints Using ASTM A325 or A490 Bolts*, Chicago.

Sabelli, R. (2000), "Research of Improving the Design and Analysis of Earthquake-Resistant Steel-Braced Frames," *2000 NEHRP Professional Fellowship Report*, EERI, Oakland, CA.

Tremblay, R., Degrange, G., and Blouin, J. (1999), "Seismic Rehabilitation of a Four-Storey Building with a Stiffened Bracing System," *Proceedings of 8th Canadian Conference on Earthquake Engineering*, Vancouver, B.C.

Watanabe, A. (1992), "Development of Composite Brace with a Large Ductility," *U.S.-Japan Workshop on Composite and Hybrid Structures*, San Francisco.

Watanabe, A., Hitomi, Y., Saeki, E., Wada, A., and Fujimoto, M. (1988), "Properties of Brace Encased in Buckling-Restraining Concrete and Steel Tube," *Proceedings of 9th World Conference on Earthquake Engineering*, Paper No. 6-7-4., Vol. IV, pp. 719-724, Tokyo-Kyoto, Japan.

Woodward-Clyde Federal Services (1997), "Draft Report: Develop Suites of Time Histories," *Report to SAC Joint Venture Steel Project*, Pasadena, CA.